IEEE Photonics Journal
An IEEE Photonics Society Publication

Open Access

Investigation on Reconstruction for Frequency Domain Photoacoustic Imaging via TVAL3 Regularization Algorithm

Volume 10, Number 5, September 2018

Qinglin Kong
Rui Gong
Jietao Liu
Xiaopeng Shao

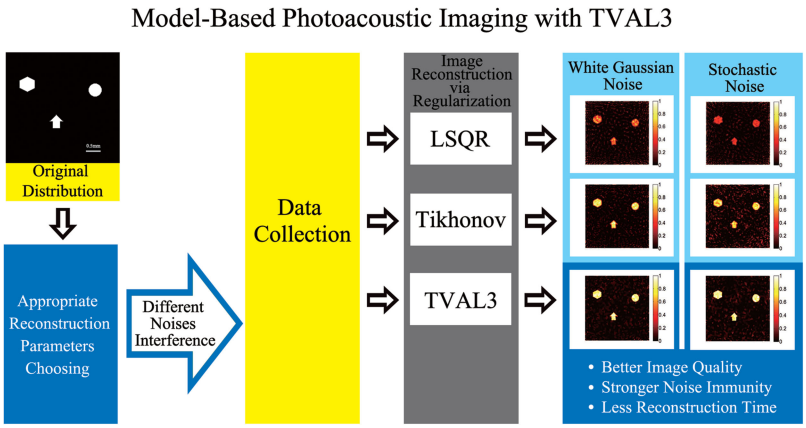

DOI: 10.1109/JPHOT.2018.2869815
1943-0655 © 2018 IEEE

IEEE photonics SOCIETY

IEEE

Investigation on Reconstruction for Frequency Domain Photoacoustic Imaging via TVAL3 Regularization Algorithm

Qinglin Kong, Rui Gong, Jietao Liu, and Xiaopeng Shao

School of Physics and Optoelectronic Engineering, Xidian University, Xi'an 710071, China

DOI:10.1109/JPHOT.2018.2869815

Manuscript received August 9, 2018; revised September 2, 2018; accepted September 6, 2018. Date of publication September 3, 2018; date of current version September 20, 2018. This study is supported by Natural National Science Foundation of China (NSFC) (61575154 & 61505156) and the 111 Project (B17035). Corresponding author: Xiaopeng Shao (e-mail: xpshao@xidian.edu.cn).

Abstract: Photoacoustic imaging (PAI) has been widely investigated by researchers from a range of areas. According to the differences between excitation laser sources, PAI can be categorized into two main types, namely the time-domain and frequency-domain PAI. Although the frequency-domain approach is more portable and economic than the other alternative, the low intensity of excitation source may lead to a lower signal-to-noise ratio (SNR). This paper aiming to propose the suitable scheme for image reconstruction, we focus on the model-based PAI system and make great efforts to reduce the impact of noise algorithmically. Three regularization algorithms, i.e., Least Square QR-factorization, Tikhonov, and Total Variation minimization by Augmented Lagrangian and alternating direction algorithms (TVAL3) are studied. By choosing three important parameters as criteria, i.e., the peak SNR, image quality index, and time consumption during different situations, the most effective regularization algorithm amongst has been selected. Based on simulation results and detailed discussions, TVAL3 algorithm performs better than the other two for model-based signal reconstruction. The result is pivotal for effective PAI in high quality and highly efficient biomedical tomography and microimaging.

Index Terms: Photoacoustic imaging (PAI), imaging parameters, regularization algorithms, white Gaussian noise (WGN), stochastic noise (SN).

1. Introduction

Photoacoustic imaging (PAI) is a new biomedical imaging technology which builds upon the foundation of photoacoustic effect. When biological tissue absorbs laser energy, its thermal expansion produces pressure waves that can be probed by ultrasonic detector in the form of ultrasound wave. Taking ultrasound wave as an information carrier makes PAI competitive to other traditional optical imaging technologies since it combines the advantages of both high penetration depth for acoustic imaging and high contrast ratio for optical imaging [1]–[4]. This technique has been successfully applied in vitro and vivo imaging of viable tissues [5], [6] and has made great strides in various biomedical applications, i.e., monitoring oxyhemoglobin saturation [7], [8], cerebral functional imaging [9] and tumor detection [10]. Currently, most of PAI systems employ nanosecond pulse lasers to stimulate the tissue for photoacoustic signals (PAS) generation. Some research uses low-energy pulse laser devices, such as diodes, as excitation sources [11]. Time domain photoacoustic signals

and noises are easier to recognize on account of the high energy density of pulse laser signals within short time duration. As a result, the noise can be easily reduced by a simple modified wavelet shift-invariance threshold would be sufficient for noise reduction for time domain PAI in most instances [12], [13].

However, the wide implementations of high energy pulse lasers in clinical applications are still challenging because of their high expense and large size. Therefore, the frequency domain PAI employing continuous wave (CW) lasers receives more attention recently. The frequency domain PAI alternatively uses near infrared CW laser as the excitation source and periodic amplitude modulations are applied onto the laser beam to generate PAS. Beyond its better portability and lower cost compared with the time domain one, frequency domain PAI owns the merits of deeper imaging depth, less harmful to operate, etc. [1], [14]–[16]. The frequency modulated photoacoustic signals can be collected to reconstruct images by corresponding reconstruction algorithms [17]–[19].

Despite of the great progress in the probing technology over the past decades, novel signal analysis methods remain highly desired for the critical demand of noise reduction in particular for the signals that too weak to be recognized after denoising by simple methods. Therefore, acquiring valuable information and filtering undesired one from a mixed signal remains a big challenge in the field of frequency domain PAI. In 2002, Paltauf's group reported an iterative algorithm to minimize the detection error [20]. Liao proposed a new way to extract the weak PAS due to diffraction with synthetic aperture focusing technique and coherence weighting [21], Wavelet denoising technic were also involved as the solution to automatic noise reduction by Holan and Viator [22]. Some other attempts are also made by other researchers worldwide [23]–[26]. Compared with that in time domain PAI, frequency domain PAS produced by the low energy-density source are even weaker and under most conditions these signals are submerged in complex noises, which make it tough or even impossible for processing reconstructions directly.

The traditional frequency domain PAI using chirp signal as its excitation signal is reconstructed with the back-projection algorithm based on Radon transform. However, back projection algorithm is a time domain signal processing path which requires huge data-collecting time and strong calculation capacity of hardware. In order to eliminate the above drawbacks, Pouyan *et.al* invented a remarkable PAS reconstruction technique which is referred as the model-based technique [27]. This method employs discrete frequency components as the excitation signal and promotes the imaging efficiency and feasibility of frequency domain PAI. Nevertheless, being a frequency domain approach, the power intensity of PAS is still weaker than that from the time domain PAI. Also, on account of the characteristic of model-based PAI, solving the ill-posed functions for the image matrix is a critical step in reconstruction. This is a very time-consuming process which may bring damage to the quality of reconstructed image by a large extent. Therefore, an optimized regularization algorithm will improve the image quality and shorten the reconstruction time. Moreover, based on our experience under the model-based PAI frame, regularization algorithms are also crucial in noise-reduction. As a result, efficient algorithms with high performance and robust operation property are desired.

In this paper, we compare the performance of three regularization algorithms, i.e., Least Square QR-factorization (LSQR), Tikhonov and Total Variation minimization by Augmented Lagrangian and alternating direction algorithms (TVAL3) in model-based PAI reconstructions. By setting up the model and programming of the simulative algorithm, detailed comparisons and analyses are conducted. Finally, we proposed several potential strategies for further improvement of model-based reconstruction of frequency domain PAI. These research results will be used as a guide for our further experiments.

2. Methods

2.1 Main Idea

In this study, the results and running time for different algorithms were investigated without considering noise in simulations at first. Then different algorithms were used under two types of noisy

circumstance. Based on the simulation, we will be able to select the best regularization algorithm for model-based PAI amongst on account of its good noise immunity, high efficiency and satisfying reconstruction results.

In this paper, the analysis is based on the model-based PAI. This type of PAI employs CW lasers as excitation source and the simulation setup is similar to the traditional frequency domain experiments. The frequency photoacoustic imaging system is normally excited by an amplitude modulated near-infrared CW laser, with a dual-channel function generator to produce modulation waveform (discrete frequency signal components). Another channel generates a pulse signal to trigger itself for synchronization. The laser beam is then collimated by a single mode fiber collimator and conducted onto sample surface. In addition, in practical applications, the samples and ultrasonic sensors should be placed in deionized water for ultrasonic coupling to reduce the loss of ultrasonic signals during its propagation. The sample is activated by the laser energy to cause thermal elastic expansion for the production of ultrasonic wave, which is also known as the PAS. The PAS are received and detected by the ultrasonic sensor. The frequencies of the signal components and the center frequency of the ultrasonic sensor are determined later in terms of the size of samples. After the collection of amplitude and phase information from the above process, we will use the following algorithm for image reconstruction in simulation.

2.2 Model-Based Frequency Domain PAI

The main process of model-based PAI is conducted as follows [27]. Assuming a point sensor is placed at the circumference of a circle which has a radius of r_d and the center is placed at point O. n measurements are taken equally spaced around. The target is placed at a spot with a distance r_0 from the center of the circle. The whole imaging area has been segmented into V square mesh grids and the distance between two neighboring grid centers is d. Derived from the wave equation in frequency domain, the acoustic wave pressure in a spatial point with modulated frequency ω can be represented as in Eq. (1).

$$\mathbf{P}(\omega) = \mathbf{W}(\omega)\mathbf{X} \tag{1}$$

$\mathbf{P}(\omega)$ is a column vector and each element is a complex number taken from n detection positions. $\mathbf{X}$ is also a column vector consisting of non-negative real numbers which represents the product of optical absorption coefficient and locally absorbed energy $\mu_a\phi(\boldsymbol{r}, \omega)$. $\mathbf{W}(\omega)$ is a matrix with $n \times V$ complex weighting factors. As a result, it can be expressed by Eqs. (2) and (3).

$$\mathbf{W}(\omega) = -j\frac{\beta}{C_p}e^{j\phi_\alpha}\begin{pmatrix} w_{11} & \cdots & w_{1V} \\ \vdots & \ddots & \vdots \\ w_{n1} & \cdots & w_{nV} \end{pmatrix} \tag{2}$$

$$w_{NV} = \omega\frac{e^{j[(\omega/c)|\boldsymbol{r}(V)-\boldsymbol{r}_d(n)|]}}{|\mathbf{r}(V) - \mathbf{r_d}(n)|} \tag{3}$$

The position of the nth detection is $\mathbf{r_d}(n)$, the position of voxel is $\mathbf{r}(V)$. Then the forward model of imaging can be written as in Eqs. (4)–(6).

$$\bar{\mathbf{P}} = \bar{\mathbf{W}}\mathbf{X} \tag{4}$$

$$\bar{\mathbf{P}} = \begin{pmatrix} \mathbf{P}(\omega_1) \\ \vdots \\ \mathbf{P}(\omega_N) \end{pmatrix} \tag{5}$$

$$\bar{\mathbf{W}} = \begin{pmatrix} \mathbf{W}(\omega_1) \\ \vdots \\ \mathbf{W}(\omega_N) \end{pmatrix} \tag{6}$$

where ω_n is the modulation frequency of the nth component. The imaging process is then simplified into solving for $\mathbf{X}$ from a system of linear equations. It obviously involves solutions for ill-posed functions where regularization algorithms are necessary. In order to accomplish such reconstruction, some techniques should be applied to optimize the accuracy and reduce the distortion of different types of noises.

Due to the low Signal to Noise Ratio (SNR) of PAS in the frequency domain PAI, the reconstructed image ofmodel-based PAI is seriously distorted under practical circumstances. Therefore, the stable solution of the ill-posed imaging matrix and noise-reduction are crucial in PAS processing. An effective regularization algorithm identifies undistorted information while solving both problems. Furthermore, the time-consumption of the imaging process is also an important evaluation criterion in practice. Therefore, the reconstruction speed of regularization is taken into consideration as well.

3. Regularization Algorithms

3.1 LSQR Algorithm

LSQR algorithm was first proposed in 1982 [28] and has become a conventional theory in solving the ill-posed problems. There are three main technics used in this algorithm, namely Lanczos iteration, orthogonal transformation and modeling iteration. LSQR converges quickly in the iterative process and its concurrent calculation can be achieved easily. As a result, this method has been used in a wide range of fields. Since this algorithm is famous for solving ill-posed problems, we will not give a detailed introduction of it in this subsection.

3.2 Tikhonov Algorithm

Tikhonov [29] algorithm is used by Pouyan when the model-based algorithm is introduced for the first time [27]. This algorithm can be treated as a reference in order to evaluate the advantages and disadvantages of other algorithms more directly.

To solve for $\boldsymbol{x}$ in the $\boldsymbol{A}\,\boldsymbol{x} = \boldsymbol{b}$ form, $\boldsymbol{x}$ can be expressed as in Eq. (7).

$$\boldsymbol{x} = \min \left\{ \|\boldsymbol{A}\,\boldsymbol{x}_\lambda - \boldsymbol{b}\|_2^2 + \lambda \|\boldsymbol{x}_\lambda\|_2^2 \right\} \tag{7}$$

where λ is the regularization parameter. The appropriate choice of λ is the decisive factor for the validity of the regularization. The core of this algorithm is to find the compromising point between the norm of solution and the norm of residue. This point represents the optimized regularization parameter. Based on the Tikhonov regularization $\boldsymbol{X}$ can be solved. This regularization method has the basic idea of singular value decomposition (SVD) involved. As has been testified by our group, the performance of Tikhonov regularization is very similar to other SVD process involved algorithms.

3.3 TVAL3 Algorithm

TVAL3 is proposed by Chengbo Li around 2010 [30], [31]. And the basic form can be expressed in Eq. (8).

$$\min_{\boldsymbol{u}_i, \boldsymbol{x}} \boldsymbol{L}_A(\boldsymbol{u}_i, \boldsymbol{x}, \boldsymbol{\gamma}_i, \beta_i, \lambda, \mu) = \min_{\boldsymbol{u}_i, \boldsymbol{x}} \sum_i \left(\|\boldsymbol{u}_i\|_p - \boldsymbol{\gamma}_i^T(\boldsymbol{D}_i\boldsymbol{x} - \boldsymbol{u}_i) + \frac{\beta_i}{2} \|\boldsymbol{D}_i\boldsymbol{x} - \boldsymbol{u}_i\|_2^2 \right) - \lambda^T(\boldsymbol{A}\,\boldsymbol{x} - \boldsymbol{y}) + \frac{\mu}{2} \|\boldsymbol{A}\,\boldsymbol{x} - \boldsymbol{y}\|_2^2, \tag{8}$$

Where $\boldsymbol{L}_A(\boldsymbol{u}_i, \boldsymbol{x}, \boldsymbol{\gamma}_i, \beta_i, \boldsymbol{\lambda}, \mu)$ is the Augmented Lagrangian Function (ALF), $\boldsymbol{u}_i$ is the slack variable, γ and λ are the Lagrangian multiplier, β and μ are the penalty factor. The procedure of TVAL3 is as follows.

1) Initialize all parameters (including $\boldsymbol{u}_{i,0}$, $\boldsymbol{x}_0$, $\boldsymbol{\gamma}_{i,0}$, $\beta_{i,0}$, $\boldsymbol{\lambda}_0$, μ_0) for i.
2) Applying augmented Lagrangian method (ALM) and alternating direction method (ADM) to find the minimum of $\boldsymbol{L}_A$ by iterative process. The iteration will only be terminated when meet one of the following criteria, which is $\|\nabla \boldsymbol{L}_A(\boldsymbol{u}_{i,k}, \boldsymbol{x}_k)\|_2$ or $\|\boldsymbol{x}_{k+1} - \boldsymbol{x}_k\|_2$ is small enough.
3) Use non-monotone line search to judge and correct the Barzilai–Borwein step length to ensure the convergence of the one step steepest descent method.
4) Continue the $k+1$th iteration unless either of the terminating criteria is satisfied in the kth iteration (k is a positive integer).

TVAL3 algorithm has been used widely in compressed sensing. It is based on the total variation regularization model and uses ALM and ADM to find the solution. ALM is usually used when solving optimization problems under equality constraints. As is known, Lagrange method can only ensure a solution to the necessary and sufficient conditions when the function is convex. Compared with the plain Lagrange method, ALM increases the robustness of dual ascent method and the strong convex constraints of the original function. Moreover, by applying ADM, the original problem is transformed into finding the solutions for two sub-problems. Referring back to Eq. (8), ADM tries to find x and u iteratively by finding $x$first then finding u subsequently in each iteration. Furthermore, to promote the calculation efficiency, TVAL3 uses Hadamard matrix as the measurement matrix. Hadamard matrix is famous for its fast transformation. In this article, we will demonstrate its utility in model-based PAI simulation.

4. Simulation Experiments and Analysis

In order to testify the feasibility and efficiency of these three algorithms, simulations with different calculation principles are presented and discussed firstly in this section. All simulations are carried out in the MATLAB environment on a Dell computer with 16 G memory and 2.8 GHz CPU. Peak Signal to Noise Ratio (PSNR) and Image Quality Index (IQI) [32] are brought in as criteria of reconstruction result quality.

PSNR is a full-reference image quality assessment criterion. It is the ratio between the maximum signal power and the noise power. The greater the PSNR value is, the less distortion the reconstruction images will be. In a 2-D imaging process, the PSNR is defined as in Eq. (9).

$$PSNR = 10 \times \log_{10}\left(\frac{(2^n - 1)^2}{MSE}\right) \tag{9}$$

Where n is the number of bits of each sampling value, in the following calculation, we take $n = 8$, MSE is the mean square error between the contaminated reconstruction image and the original distribution and is defined by Eq. (10).

$$MSE = \frac{1}{hw}\sum_{i=1}^{h}\sum_{j=1}^{w}\left\|I(i,j) - K(i,j)\right\|^2 \tag{10}$$

Where h is the height of the images in number of pixels, w is the width of the images in number of pixels. $I(i,j)$ is the value of the pixel in ith row and jth column in the original distribution, and $K(i,j)$ is the value of the corresponding pixel in the reconstructed image.

PSNR is widely applied in a variety of fields. Although sometimes the value of PSNR is not completely coincident with the subjective visual feelings of humans, from the computational formula of PSNR we can easily recognize that this assessment criterion is objective enough for an impartial evaluation. Besides, this parameter is very straight forward to understand and that is the reason why it is chosen as the first assessment criterion.

IQI is more widely known as structure similarity index (SSIM) index and can be expressed by Eq. (11).

$$IQI = \frac{4\sigma_{xy}\bar{x}\bar{y}}{\left(\sigma_x^2 + \sigma_y^2\right)\left[(\bar{x})^2 + (\bar{y})^2\right]} \tag{11}$$

In case the denominator might be 0 and cause trouble for calculation, some constants would be added and the original expression can be expressed in the form of Eq. (12).

$$IQI = \frac{(2\bar{x}\bar{y} + C_1)(2\sigma_{xy} + C_2)}{\left(\sigma_x^2 + \sigma_y^2 + C_1\right)\left[(\bar{x})^2 + (\bar{y})^2 + C_2\right]} \tag{12}$$

We normally take $C_1 = 0.01L$, $C_2 = (0.03L)^2$ in practice, L is the image gray scale level. $\bar{x}$ and $\bar{y}$ is the mean value of image x and$y$, σ_x^2 and σ_y^2 is the variance of image x and$y$, σ_{xy} is the covariance between image x and$y$, the parameters can be calculated by Eqs. (13) to (17).

$$\bar{x} = \frac{1}{hw}\sum_{i=1}^{h}\sum_{j=1}^{w} x(i,j) \tag{13}$$

$$\bar{y} = \frac{1}{hw}\sum_{i=1}^{h}\sum_{j=1}^{w} y(i,j) \tag{14}$$

$$\sigma_x^2 = \frac{1}{hw-1}\sum_{i=1}^{h}\sum_{j=1}^{w} [x(i,j) - \bar{x}]^2 \tag{15}$$

$$\sigma_y^2 = \frac{1}{hw-1}\sum_{i=1}^{h}\sum_{j=1}^{w} [y(i,j) - \bar{y}]^2 \tag{16}$$

$$\sigma_{xy} = \frac{1}{hw-1}\sum_{i=1}^{h}\sum_{j=1}^{w} [x(i,j) - \bar{x}][y(i,j) - \bar{y}] \tag{17}$$

where h is the height of the images in number of pixels, w is the width of the images in number of pixels. $x(i,j)$ is the value of the pixel in ith row and jth column in the original distribution, and $y(i,j)$ is the value of the corresponding pixel in the reconstructed image.

Compared with the PSNR, IQI is a more full-scale image quality assessment factor. It takes brightness distortion, contrast distortion and structural distortion into consideration to give a more comprehensive assessment. Therefore, IQI is selected as the second image quality assessment criterion. The closer the IQI is to the 1, the less distortion is contained in the reconstruction image.

The diameter of the sample object corresponds to a particular spatial frequency and can be calculated as in Eqs. (18) and (19).

$$t = \frac{d}{c} \tag{18}$$

$$f_s = \frac{1}{t} = \frac{c}{d} \tag{19}$$

Where d represents the diameter or characteristic dimension of the sample object, c is the speed of sound within the tissue. Throughout the simulation, we take $c = 1500$ m/s. f_s is the lower bound of the modulated frequency in order to accurately analysis the scale of the sample object. In other words, only if the frequency components are greater than the lower threshold can the sample be accurately distinguished from the environment. Comparing with the chirp signal excitation mode, discrete frequency modulation mode only need to record a complex number which contains the amplitude and phase information of PAS rather than restore all the data for later image processing.

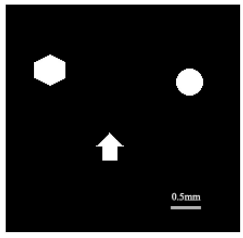

Fig. 1. Original distributions of the sample.

The difference between the data volume can dramatically reduce the memory space of the computer and improve the calculation speed dramatically.

The original distribution has been shown in Fig. 1. There are three target objects in this sample, a circle, an arrow and a hexagon, and their scales are about 0.5 mm. The absorption coefficient for all objects is 1 and the absorption coefficient for the dark area is 0. In Fig. 1, the grey scale of the target is 255 and the grey scale of the background area is 0. As a result, the optical contrast of the original distribution is 1. According to Eqs. (18) and (19), the lower frequency threshold is approximately 3 MHz.

4.1 Selecting Appropriate Simulation Parameters

For a convincing simulation analysis, proper selection of parameters is a crucial factor. There are several critical parameters for successful simulation, such as the number of detecting angels around the perimeter of detector trajectory, the number of frequency components N and the bandwidth BW of the frequency domain. For now, we will take the number of detecting angels to be 50 through the simulation for convenience, which is equivalent of taking observation every 7.2 degrees around the circular trajectory of detector in experimental environment (the excitation source moves with the detector, and the relative position between detector and excitation source remains unchanged all throughout the whole data collecting process).

On each of the 50 observation positions, N frequency components are utilized for signal generation. The Ncomponents are equally spaced within the frequency range of BW, and the first frequency component equals to the lower bond of the frequency range and the last one equals to the upper bond of the frequency range. For example, if we take the BW range from 0 to 10 MHz and chose 101 frequency components, the first frequency component should be 0Hz and the last one should be 10 MHz, and the step size is 0.1 MHz. As the BW is always given explicitly in this subsection, the step size of frequencies will be indicated in brackets.

First of all, we are going to explore the influence of different numbers of frequency components N for reconstruction. The BW for Fig. 2 is from 0 to 10 MHz, we take 2 (step size 10 MHz), 21 (step size 0.5 MHz), 51 (step size 0.2 MHz) and 101 (step size 0.1 MHz) components from each observation position.

Reconstruction results in each column have the same N while the results in each row are reconstructed by the same regularization algorithm. As can be visualized clearly in Fig. 2, for the same regularization algorithm, increasing the number of frequency components can definitely improve the quality of the PAI. When $N = 2$, the information is far from sufficient for a successful reconstruction. When $N = 21$, these results are mixed up with severe artificial noises and the information is still insufficient for the LSQR and Tikhonov scheme to recover the details of the original sample objects. Especially the Tikhonov reconstruction results, even the shape of the sample objects have been distorted. When $N = 51$, only small artificial noises exist in the results of LSQR scheme, while the reconstructed images for all three algorithms are neat and clean for all three schemes when $N = 101$. Meanwhile, when the number of frequency components is fixed, the TVAL3 algorithm can always give the best results except for when $N = 2$, under which circumstance the PAI quality is too poor as a meaningful comparison. Table 1 shows the time consumption for each simulation in Fig. 2. The unit for time consumption is in second.

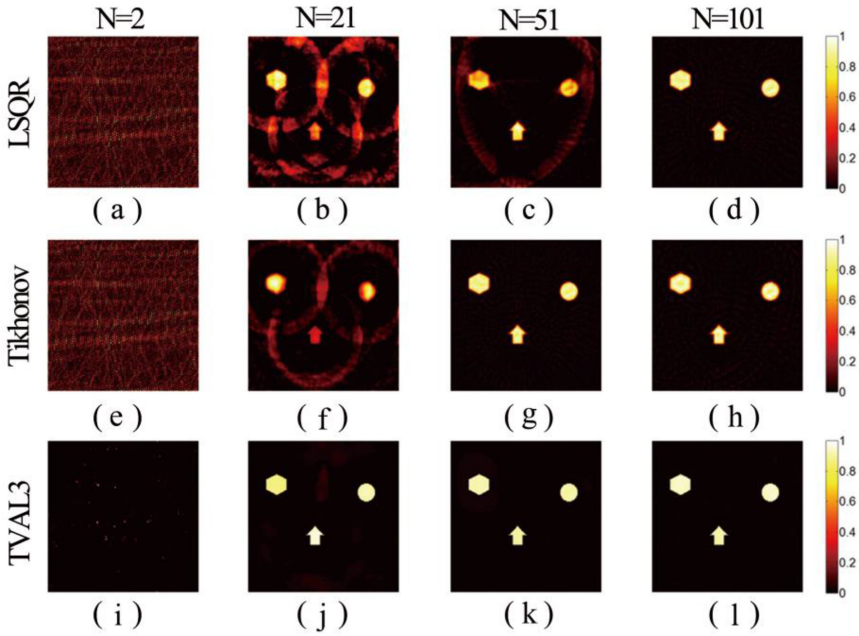

Fig. 2. Reconstruction results with different number of frequency components.

TABLE 1
Running Time (s) for Reconstruction of Fig. 2

Algorithm	N=2	N=21	N=51	N=101
LSQR	2.09	25.14	100.84	451.07
Tikhonov	0.77	18.49	114.07	659.84
TVAL3	7.17	28.65	51.3	100.08

When N is very small, TVAL3 scheme takes the longest time for solving for the image. As N increases and the image quality improves, time consumption for TVAL3 algorithm rises very slowly while there are sharp increments for the other two group of imaging algorithms. When $N = 101$, TVAL3 only takes about 22% and 15% running time of LSQR and Tikhonov respectively, which is extremely efficient.

Different BW values also vary the reconstruction results. In the following part of this sub-section, we will take $N = 51$ and investigate the impact of different BW values.

Figure 3 shows the reconstruction results for different parameters of BW. When BW is between 0–2.5 MHz (step size 0.05 MHz), the upper threshold is lower than 3 MHz, all the imaging results in (a), (d), (g) lose some of the details of the three sample objects, and their edges become blurred and even distorted, especially for the arrow. When BW is between 0–5 MHz (step size 0.1 MHz), the results of the three PAIs almost restored every detail in Fig. 1. Furthermore, it is obvious that the TVAL3 scheme gives the best result since its absorption coefficient is very similar to the original distribution. From the previous analysis of different N values, increasing the number of frequency component while keeping BW constant will improve the image quality. However, it is not correct vice versa.

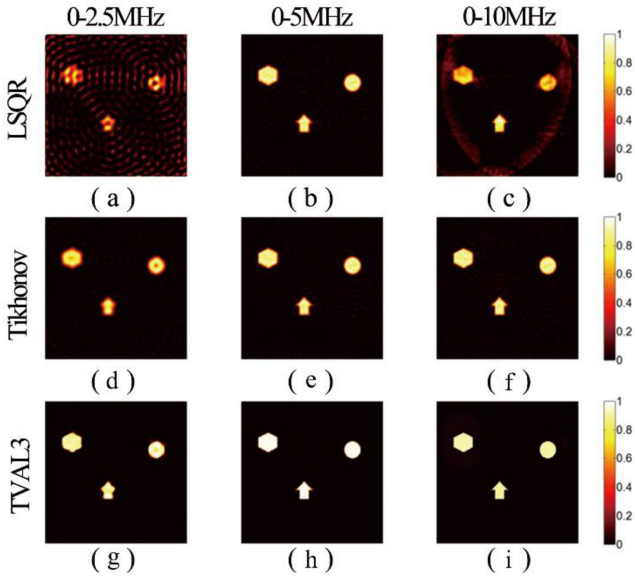

Fig. 3. Reconstruction results under different excitation bandwidths.

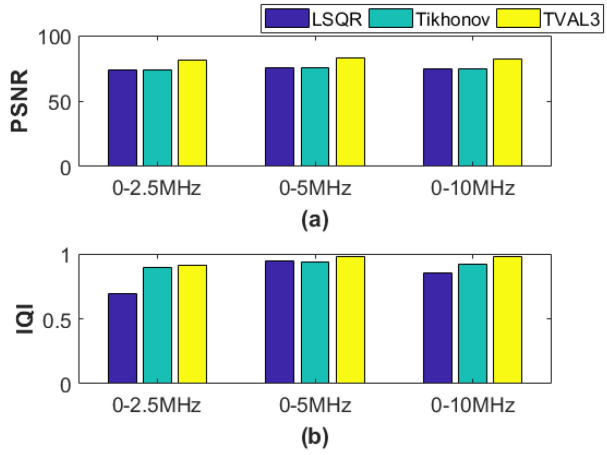

Fig. 4. Quality parameters for reconstruction results under different BW values.

The quality plots for different BW values are shown in Fig. 4. The qualities of the images increase first when the BW value is extended from 2.5 to 5 MHz, but decreases as the further increase to 10 MHz of BW (step size 0.2 MHz). It is due to the fact that along with the increase of BW, more noises are brought in with more information. When the BW values increase gradually, the augment of information becomes slower and less obvious. There will be a threshold point whose benefits are lower than the loss by widening BW. In other words, impact of noises increases faster than that of information, which will definitely damage the image quality.

Table 2 shows the time consumption for each simulation in Fig. 3. The results reveal the same trend as it could be shown in Table 1. That is when N is sufficient for a quality reconstruction, TVAL3 is the most efficient and effected choice for the best quality reconstruction. The image quality of LSQR results is a bit worse than that of the Tikhonov results, while Tikhonov results take a bit longer time. We should also notice that, when N is fixed, the reconstruction time for each algorithm only varies in a very small range because the size of observation matrix are constant. We may

TABLE 2
Running Time (s) for Reconstruction of Fig. 3

Algorithm	BW=0-2.5MHz	BW=0-5MHz	BW=0-10MHz
LSQR	110.6	107.22	100.84
Tikhonov	121.53	123.19	114.07
TVAL3	48.16	49.89	51.3

not be able to infer the accurate running time for each algorithm during other simulations and even the practical applications, but this fact should be very useful to estimate relative imaging speed of these three algorithms in discrete frequency PAI. We will testify the validity of this inference in the following sections.

We also investigate the situation if the center of excitation frequency changes while N and BW are both kept constant. The results reveal that, as the center of frequency increases, the edges of each sample objects become sharper. Meanwhile, the information for the blocks gets lost gradually. It is expected as same as common sense, in this paper we will not present these results for conciseness.

Based on the analysis in this subsection, in further simulations, we choose $N = 51$ and BW is from 0 to 5 MHz. Or in other words, the frequency components in each position are 0 Hz, 0.1 MHz, 0.2 MHz, 0.3 MHz, . . . , 4.8 MHz, 4.9 MHz and 5 MHz. The size of all reconstruction images is 216×210 pixels and the distance between vertically/horizontally adjacent pixels is 20 μm.

4.2 Simulation With Different Types Of Noises

For a convincing simulation analysis, proper selection of parameters is a key factor. There are several critical parameters for successful frequency domain PAI reconstruction.

In the experimental environment, these are two main types of noises possibly interfering with the PAS. In this sub-section, noises of White Gaussian Noise (WGN) and Stochastic Noise (SN) are investigated.

The amplitude of WGN is normally distributed in the time domain and the power of WGN is uniform throughout the frequency domain. In practice, the noises generally come from multiple sources. Suppose the real noise can be considered as the sum of the environment, many applications of random variables, and each of the random variables is independent. Their normalized sum will tend to be a Guassian distribution as the quantity of noise sources according to central limit theorem. When the origin of noises is very complex and we have no explicit idea of where the noises come from, WGN is a very simple and reasonable choice for mimicking the real-world-noises in simulations.

However, WGN is not optimal choice for all situations. If the quantity of source is very limited or more than a certain number of individual noises are extremely strong, WGN may not work very well. In this case, we introduce SN for simulation. SN is a series of random numbers with a certain amplitude average. SN is even more flexible than WGN and can increase the generality of simulation.

We take four different WGNs with SNR 10 dB, 0 dB, -10 dB and -20 dB respectively. Firstly, we choose only one group of WGN for simulation.

Figure 5 shows reconstruction results under WGN with different levels of SNRs. Since the differences between LSQR and Tikhonov algorithms under relatively low WGN levels are not obvious. We also have the PSNR and IQI of each image plotted for better comparisons. Figure 6 gives a clear view of the image quality of three different algorithms under different WGN levels.

The intensity of WGN we use actually ascends quickly. However, the deterioration of the image quality is very slow, except for the LSQR scheme when the noise becomes very strong.

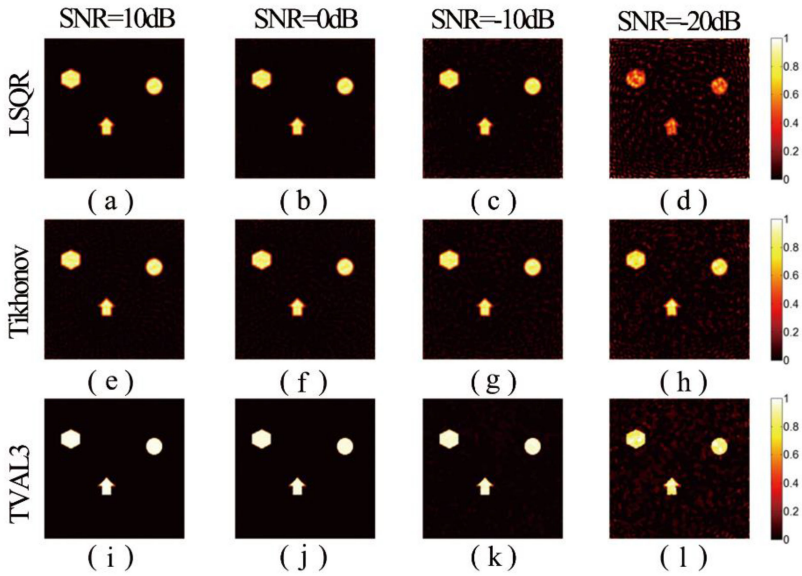

Fig. 5. Reconstruction results under different SNR levels of WGNs.

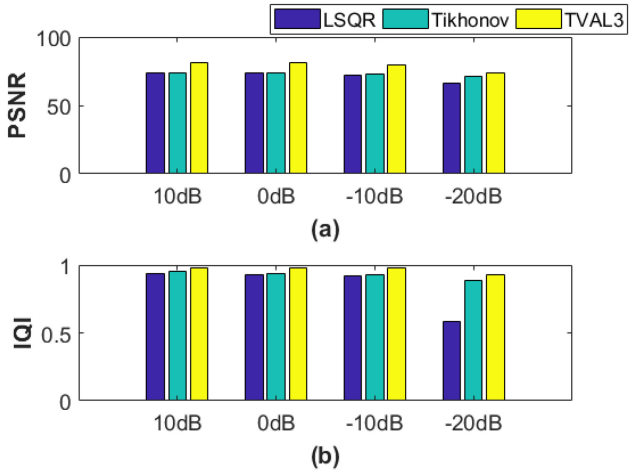

Fig. 6. Quality parameters for reconstruction results under different levels of WGNs.

As has been demonstrated before in Section 4.1, the time consumption for the same regularization algorithm are very similar under different situation if the original distribution, N and BW remain unchanged. This inference has been testified here, the running time is shown in Table 3. TVAL3 is still the most effective and efficient algorithm under WGN.

It is noted that although TVAL3 always gives the best reconstruction results according to both of the image quality criteria, the WGN noise cannot be eliminated especially when the SNR becomes really high. In practice, we can eliminate the WGN by taking many groups of measurements. By finding the average of the observation data set and detracting the average noise intensity (we normally use a constant for approximation) we can eliminate the influence of WGN. For example, we take 50 measurements and follow the normal WGN elimination process, and the results are presented in Fig. 7.

TABLE 3
Running Time (s) for Reconstruction of Fig. 5

Algorithm	WGN=10dB	WGN=0dB	WGN=-10dB	WGN=-20dB
LSQR	107.98	106.97	106.93	105.15
Tikhonov	117.2	118.25	115.46	119.04
TVAL3	47.58	50.1	49.04	54.96

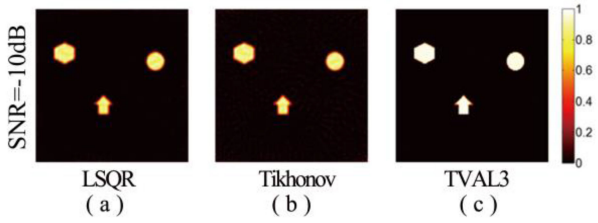

Fig. 7. Reconstruction results by applying WGN elimination process.

The WGNs have been reduced sharply so that the image quality has been improved a lot by following the normal WGN elimination process. However, it does not imply that study on functionality of regularization schemes to WGN is meaningless. We take the −10 dB situation as an example, if we want to achieve 95% quality level of the no-noise situation, LSQR needs about 52 groups of measurements, and Tikhonov needs about 46 groups of measurements, while TVAL3 only needs about 27 groups of measurements. It is worth clarifying that using the term “about” is because we conducted investigation on each algorithm for 10 times, group number varies a bit from time to time. The results are the average for those 10 times. This can definitely promote the productivity in the future practical application.

The impacts of SNs are also shown in this sub-section. We take three different SNs with SNR 5 dB, 0 dB and −5 dB respectively. Figure 8 shows reconstruction results under SN with different levels of SNRs. For a more intuition comparison, the PSNR and IQI of each image are plotted in Fig. 9.

Figure 9 shows the image quality factors of all reconstructions. The quality factors for reconstruction results under WGN degrade very slowly along with the rapid growth of noise level. Nevertheless, the images lose their quality very fast under SN even if the increase of noise intensity is much slower than those under the WGN situations.

From Figs. 7 and 9, the TVAL3 algorithm always gives the best reconstruction qualities and Tikhonov algorithm gives the second best results all through. Both of these two algorithms have relative good noise immunity whereas TVAL3 performs much better than Tikhonov. Reconstruction qualities by LSQR vary with different levels of noises, the qualities of the results are very close to the Tikhonov algorithm, but the degrading becomes very severe when the noises grow very strong.

Table 4 shows the reconstruction time range for different images. Our inference in Section 3.1 has again be testified. The TVAL3 algorithm is still the most efficient algorithm under all conditions. Tikhonov and LSQR algorithms consume about the same time lengths during all simulations.

From the simulations in this section, TVAL3 algorithm is without doubt the most effective and efficient regularization scheme regardless of the existence of and the types of noise. On account of the application of those methods, the efficiency, robustness and flexibility of TVAL3 are much better than the other two regularization algorithms. Its rapid arithmetic speed, strong anti-noise ability, parameter-insensitivity and feasibility for various measurement matrixes under complex situations make it a very promising solution in future applications for model-based frequency domain PAI. The merits of TVAL3 algorithm mentioned in Section 3.3 have been thoroughly verified through simulations.

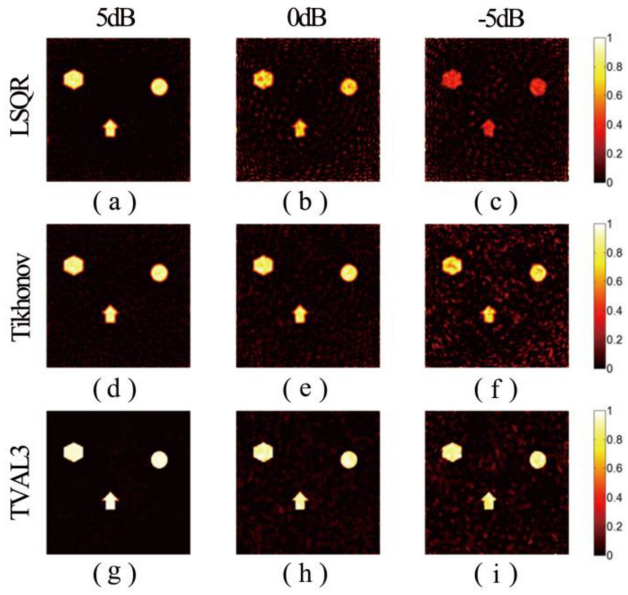

Fig. 8. Reconstruction results under different SNR levels of SNs.

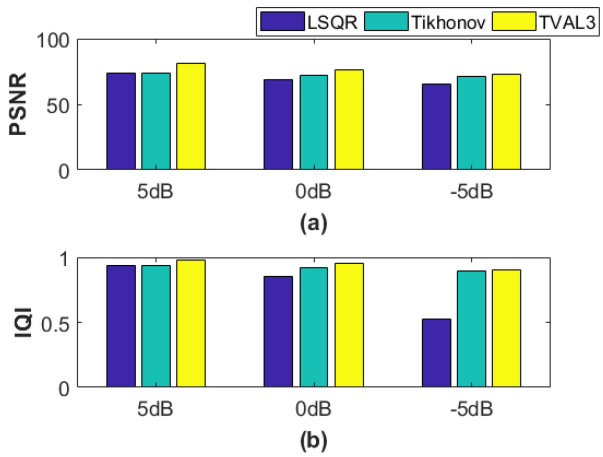

Fig. 9. Quality parameters for reconstruction results under differnt levels of SNs.

TABLE 4
Running Time (s) for Reconstruction of Fig. 8

Algorithm	WGN=10dB	WGN=0dB	WGN=-10dB
LSQR	107.98	106.97	106.93
Tikhonov	117.2	118.25	115.46
TVAL3	47.58	50.1	49.04

5. Conclusion

In this study, the efficiency of three regularization algorithms for model-based PAI reconstruction are investigated and analyzed numerically. By conducting study under different circumstances with different parameters, the relative efficiencies of different algorithms are concluded to be stable in most cases. Among these three schemes, the results show that the optimal solutions are achieved with TVAL3 all through. Tikhonov can give better-quality images in contrast to LSQR but consume a bit more time in reconstruction. Whereas TVAL3 always turn out to be the fastest regularization algorithm as long as the reconstruction parameters are sufficient for a satisfying reconstruction. In summary, TVAL3 is the most effective and efficient method in all the three methods investigated. The application of TVAL3 will improve the image quality and time efficiency to a great extent in PAI reconstruction. These findings will be very useful for our further experiment in the coming future.

Acknowledgment

The authors would like to thank C. Gong for the insightful discussions. The authors also wish to thank the anonymous reviewers for their valuable suggestions.

References

[1] S. A. Telenkov and A. Mandelis, "Photothermoacoustic imaging of biological tissues: Maximum depth characterization comparison of time and frequency-domain measurements," *J. Biomed. Opt.*, vol. 14, no. 4, 2009, Art. no. 044025.
[2] A. Rosencwaig and A. Gersho, "Theory of photoacoustic effect in solids," *J. Appl. Phys.*, vol. 47, no. 1, pp. 64–69, 1976.
[3] D. Huang *et al.*, "Optical coherence tomography," *Science*, vol. 254, no. 5035, pp. 1178–1181, 1991.
[4] H. F. Zhang, K. Maslov, G. Stoica, and L. V. Wang, "Functional photoacoustic microscopy for high-resolution and noninvasive in vivo imaging," *Nature Biotechnol.*, vol. 24, no. 7, pp. 848–851, 2006.
[5] R. R. Anderson and J. A. Parrish, "The optics of human skin," *J. Investigative Dermatol.*, vol. 77, no. 1, pp. 13–19, 1981.
[6] M. I. Sereno *et al.*, "Borders of multiple visual areas in humans revealed by functional magnetic resonance imaging," *Science*, vol. 268, no. 5212, pp. 889–893, 1995.
[7] S. Zackrisson, V. D. V. Sm, and S. S. Gambhir, "Light in and sound out: Emerging translational strategies for photoacoustic imaging," *Cancer Res.*, vol. 74, no. 4, pp. 979–1004, 2014.
[8] H. F. Zhang, K. Maslov, M. Sivaramakrishnan, G. Stoica, and L. V. Wang, "Imaging of hemoglobin oxygen saturation variations in single vessels in vivo using photoacoustic microscopy," *Appl. Phys. Lett.*, vol. 90, no. 5, pp. 053901-1–053901-3, 2007.
[9] X. Wang, Y. Pang, G. Ku, X. Xie, G. Stoica, and L. V. Wang, "Noninvasive laser-induced photoacoustic tomography for structural and functional in vivo imaging of the brain," *Nature Biotechnol.*, vol. 21, no. 7, pp. 803–806, 2003.
[10] R. A. Kruger, R. B. Lam, D. R. Reinecke, S. P. Del Rio, and R. P. Doyle, "Photoacoustic angiography of the breast," *Med. Phys.*, vol. 37, no. 11, pp. 6096–6100, 2010.
[11] J. Y. Zhang, W. M. Xie, Z. P. Zeng, and L. Hui, "Recent progress in photoacoustic imaging technology," *Chin. J. Opt.*, vol. 4, no. 2, pp. 111–117, 2011.
[12] P. Kirkpatrick and A. V. Baez, "Formation of optical images by X-rays," *J. Opt. Soc. Amer.*, vol. 38, no. 9, pp. 766–774, 1948.
[13] P. Pignoli, E. Tremoli, A. Poli, P. Oreste, and R. Paoletti, "Intimal plus medial thickness of the arterial wall: A direct measurement with ultrasound imaging," *Circulation*, vol. 74, no. 6, pp. 1399–1406, 1986.
[14] A. Mandelis, "Bioacoustophotonic depth-selective imaging of turbid media and tissues: Instrumentation and measurements," in *Proc. WSEAS Int. Conf. Signal Process., Comput. Geom. Artif. Vis.*, 2006, pp. 160–169.
[15] B. Lashkari and S. Mandelis, "Comparison between pulsed laser and frequency-domain photoacoustic modalities: Signal-to-noise ratio, contrast, resolution, and maximum depth detectivity," *Rev. Sci. Instrum.*, vol. 82, no. 9, 2011, Art. no. 041101.
[16] S. Telenkov and A. Mandelis, "Signal-to-noise analysis of biomedical photoacoustic measurements in time and frequency domains," *Rev. Sci. Instrum.*, vol. 81, no. 12, 2010, Art. no. 024007.
[17] A. P. Gibson, J. C. Hebden, and S. R. Arridge, "Recent advances in diffuse optical imaging," *Phys. Med. Biol.*, vol. 50, no. 4, pp. R1–R43, 2005.
[18] S. A. Telenkov, R. Alwi, A. Mandelis, and A. I. Vitkin, "Frequency domain photoacoustic correlation (radar) imaging: A novel methodology for non-invasive imaging of biological tissues," *Proc. SPIE*, vol. 8223, no. 3, pp. 82231J-1–82231J-6, 2012.
[19] E. Lüscher, "Photoacoustic effect in condensed matter—Historical development," *Photoacoustic Effect Principles and Applications*. New York, NY, USA: Springer, 1984.
[20] L. Lin, J. Xia, T. T. W. Wong, R. Zhang, and L. V. Wang, "In vivo deep brain imaging of rats using oral-cavity illuminated photoacoustic computed tomography," in *Proc. Photons Plus Ultrasound, Imag. Sensing*, pp. 016019-1–016019-4, 2015.
[21] J. Yao, J. Xia, and L. V. Wang, "Multiscale functional and molecular photoacoustic tomography," *Ultrason. Imag.*, vol. 38, no. 1, pp. 44–62, 2015.

[22] K. J. Cash, C. Li, J. Xia, L. V. Wang, and H. A. Clark, "Optical drug monitoring: Photoacoustic imaging of nanosensors to monitor therapeutic lithium in vivo," *ACS Nano*, vol. 9, no. 2, pp. 1692–1698, 2011.
[23] B. Arnal *et al.*, "Sono-photoacoustic imaging of gold nanoemulsions: Part I. Exposure threshold," *Photoacoustics*, vol. 3, no. 1, pp. 3–10, 2015.
[24] B. Arnal *et al.*, "Sono-photoacoustic imaging of gold nanoemulsions: Part II. Exposure threshold," *Photoacoustics*, vol. 3, no. 1, pp. 11–19, 2015.
[25] S. Telenkov, A. Mandelis, B. Lashkari, and M. Forcht, "Frequency-domain photothermoacoustics: Alternative imaging modality of biological tissues," *J. Appl. Phys.*, vol. 105, no. 10, 2009, Art. no. 102029.
[26] B. Lashkari and A. Mandelis, "Comparison between pulsed laser and frequency-domain photoacoustic modalities: Signal-to-noise ratio, contrast, resolution, and maximum depth detectivity," *Rev. Sci. Instrum.*, vol. 82, no. 9, 2011, Art. no. 041101.
[27] P. Mohajerani, S. Kellnberger, and V. Ntziachristos, "Frequency domain optoacoustic tomography using amplitude and phase," *Photoacoustics*, vol. 2, no. 3, pp. 111–118, 2014.
[28] C. C. Paige and M. A. Saunders, "LSQR: An algorithm for sparse linear equations and sparse least squares," *ACM Trans. Math. Softw.*, vol. 8, no. 1, pp. 43–71, 1982.
[29] G. H. Golub, P. C. Hansen, and D. P. O.' Leary, "Tikhonov regularization and total least squares," *SIAM J. Matrix Anal. Appl.*, vol. 21, no. 1, pp. 185–194, 2000.
[30] C. Li, "An efficient algorithm for total variation regularization with applications to the single pixel camera and compressive sensing," Master's theses, Dept. Comput. Appl. Math., Rice Univ., Houston, TX, USA, 2010.
[31] C. Li, W. Yin, H. Jiang, and Y. Zhang, "An efficient augmented Lagrangian method with applications to total variation minimization," *Comput. Optim. Appl.*, vol. 56, no. 3, pp. 507–530, 2013.
[32] Z. Wang, H. R. Sheikh, and A. C. Bovik, "Objective video quality assessment," *Handbook Video Databases Design Appl.*, vol. 17, no. 5, pp. 1041–1078, 2003.